Reliability Engineering and System Safety 191 (2019) 106550

Contents lists available at ScienceDirect

Reliability Engineering and System Safety

journal homepage: www.elsevier.com/locate/ress

Fatigue reliability assessment of offshore wind turbines with stochastic availability

Jan-Tore Horn[*,a,b], Bernt J. Leira[b]

[a] Centre for Autonomous Marine Operations and systems (NTNU AMOS), NTNU, Trondheim, Norway
[b] Department of Marine Technology, NTNU, Trondheim, Norway

ARTICLE INFO

Keywords:
Offshore wind turbines
Reliability
Downtime
Fatigue

ABSTRACT

In this paper, the impact on lifetime estimation of an offshore wind turbine by introducing a stochastic model for the availability is investigated. Offshore bottom-fixed wind turbines typically have an average downtime of 4–10% due to e.g. grid- or mechanical failures including a potentially long response time for recovery. During the non-operational conditions, the fatigue damage in the foundation is accumulating significantly faster. Designing the wind farm based on a conservative downtime fraction will lead to design conservatism with respect to the foundation, which will be quantified in this paper using a structural reliability analysis.

1. Introduction

The overall costs of an offshore wind farm is highly dependent on the substructure designed to keep the turbine in place or floating in a safe and reliable manner during the operational lifetime. To date, the simplistic monopile foundation has proven to be the most cost efficient solution in water depths up to at least 40 m. In the present work, an extra large monopile foundation supporting a 10MW wind turbine is chosen as the basis for the dynamic system for which the long term structural fatigue is to be evaluated.

When moving the wind energy industry offshore to larger water depths and further away from the mainland, additional considerations must be made with respect to environmental loading from waves, currents and tides [1]. Comparing to an onshore turbine, the load situation for which the design criteria are to be met, is much more complex. Depending on the desired accuracy of the structural response and reliability estimations, the environmental loading parameters can be extended to a large number of dimensions. If design conservatism can be reduced by including extra loading parameters and stochastic descriptions, methods should be readily available for spending computational efforts to improve the system knowledge and decrease modelling uncertainties. A general method involving efficient use of idle computing resources rather than a case-optimised method is used for the present long-term analyses.

Fatigue life estimation of offshore wind turbines requires simulations of the response due to combined external loads according to design load case (DLC) 1.2 in [1]. Other load cases may also contribute to the overall fatigue damage, but DLC 1.2 is expected to be the main contributor. For an offshore wind turbine, this means to simulate with a sufficient amount of external conditions to represent the expected fatigue damage during the operational lifetime (see e.g. [2]). Due to many types of external parameters (wind, wave height, wave direction, current etc.) a full fatigue limit state (FLS) analysis may become computationally demanding. As a result, there has been an effort to develop simplified methods for quick load analysis in the frequency domain [3–5]. In addition, efforts has been made to reduce the number of load cases and total simulation length while maintaining the accuracy [6,7].

The present work uses a high dimensional joint distribution fitted to data from a likely site of a future offshore wind farm in the central North Sea. Environmental parameters include wind, wind-generated sea (wind sea), swell and tide as well as their respective directional statistics. Further, the distribution is used for generating short-term sea states in a long-term analysis of the turbine in question by means of Gibbs sampling and cluster computing. Removing the need for binning the data and finding the probability of occurrence for each sea state are some of the advantages when using a direct sampling from the joint distribution. It is also of great interest to obtain an estimation of the estimated fatigue error incorporated in the structural reliability, which only can be obtained by an analysis in the entire variable domain. Furthermore, there is no need to discretise the domain where the load effects are unknown as these will be accounted for automatically if the number of samples are sufficiently large. For instance, if the tidal parameters do not contribute to the response, the result is a faster convergence of the load effects. Finally, when the convergence criteria

* Corresponding author at: Centre for Autonomous Marine Operations and systems (NTNU AMOS), NTNU, Trondheim, Norway.
E-mail address: jan-tore.horn@ntnu.no (J.-T. Horn).

https://doi.org/10.1016/j.ress.2019.106550
Received 9 February 2018; Received in revised form 6 June 2019; Accepted 26 June 2019
Available online 27 June 2019

of the investigated response is met, sensitivity factors and response characteristics for the fatigue damage with respect to input parameters are estimated using the probabilistic analysis tool PROBAN [8].

The availability of an offshore wind turbine (OWT) is a measure of the ratio between the duration for which the turbine is unable to produce energy and the total time for possible power production. While parked, the dynamic characteristics changes significantly. For bottom-fixed OWTs the damping level is dramatically reduced, resulting in an increased fatigue damage accumulation [9]. Unless data on the actual downtime fraction is available, the availability is taken as 90 or 100%, whichever is most conservative [1]. The purpose of this paper is to reduce the potential design conservatism related to the availability parameter by means of probabilistic analysis.

The paper is built up as follows; first, the design basis including the environmental- and numerical model is presented. Second, the simulation procedures and sub-populations required to perform long-term reliability analyses are discussed. Finally, the reliability analysis is performed, with an investigation of the most dominating parameters and the impact of availability on the failure probability.

2. Offshore site and environmental model

Hindcast data for description of the wind and wave environment is provided by the Norwegian Meteorological Institute and the NORA10 database [10] for the location shown in Fig. 1. The data contains information about the wind speed, wind direction and significant wave height, peak period, and direction for both wind sea and swell. The data is valid for periods of 3 h durations and some of the available parameters are listed in Table 1 with corresponding probability distributions.

The complete environmental joint distribution is modelled as:

$$f_{\mathbf{X}_e} = f_{\mathbf{X}_w} \cdot f_{\mathbf{X}_s} \cdot f_{H_t} \tag{1}$$

where the wind sea variables are gathered in:

$$\mathbf{X}_w = [V,\ \Theta_v,\ H_S^w,\ T_P^w,\ \Theta_w^r] \tag{2}$$

where descriptions can be found in Table 1, and

$$\mathbf{X}_s = [H_S^s,\ T_P^s,\ \Theta_s] \tag{3}$$

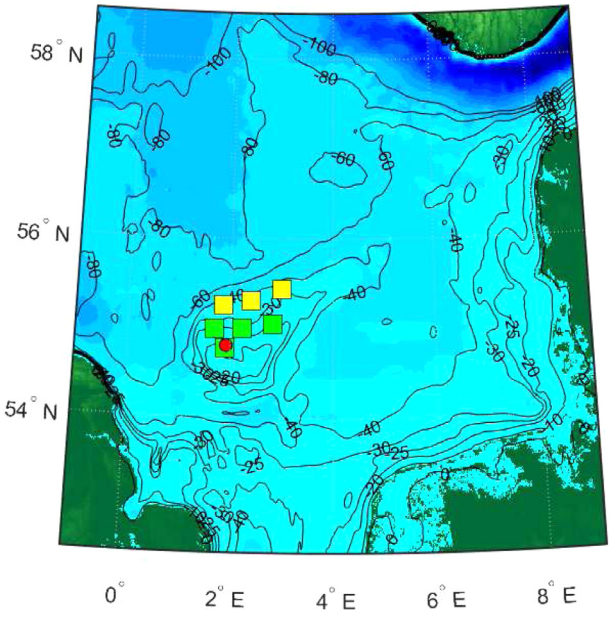

Fig. 1. Planned (green) and possible (yellow) offshore wind farms at Dogger Bank with location for hindcast data (red). (For interpretation of the references to colour in this figure legend, the reader is referred to the web version of this article.)

Table 1
Marginal distribution types and description of environmental parameters.

Parameter		Distribution	Description	Unit
V	v	3-p Weibull	Wind speed at 100 m	[m/s]
Θ_v	θ_v	von Mises mix	Wind direction at 100 m	[deg]
H_S^w	h_w	3-p Weibull	Significant wave height for wind sea	[m]
T_P^w	t_w	Lognormal	Peak period for wind sea spectrum	[s]
Θ_w^r	θ_w	Trunc. normal	Relative wind-wave direction	[deg]
H_S^s	h_s	3-p Weibull	Significant wave height for swell	[m]
T_P^s	t_s	Lognormal	Peak period for swell spectrum	[s]
Θ_s	θ_s	von Mises mix	Swell direction	[deg]
H_t	H	Normal mix	Water level	[m]

for swell. The variable dependencies are described with:

$$f_{\mathbf{X}_w} \approx f_V \cdot f_{\Theta_v|V} \cdot f_{H_S^w|V} \cdot f_{T_P^w|H_S^w} \cdot f_{\Theta_w^r|H_S^w} \tag{4}$$

for wind sea, and

$$f_{\mathbf{X}_s} \approx f_{H_S^s} \cdot f_{T_P^s|H_S^s} \cdot f_{\Theta_s|H_S^s} \tag{5}$$

for swell. The distribution types are given in Table 1 and chosen based on a previous study [11] where the von Mises distribution was found very useful for modelling directions. Furthermore, is was found that a 3-parameter Weibull distribution was necessary in order to model the wave heights accurately. A normal distribution truncated at $\pm$ 90° proved suitable for modelling the relative wind-wave direction for wind-generated sea.

3. Numerical wind turbine model

The numerical model is a bottom-fixed monopile-mounted turbine with tower and rotor-nacelle assembly (RNA) as described in [12]. To obtain a realistic natural period, the tower thickness is increased with 20% [13]. The final dimensions of the monopile and transition piece can be found in Fig. 2. The resulting first fore-aft and side-side natural

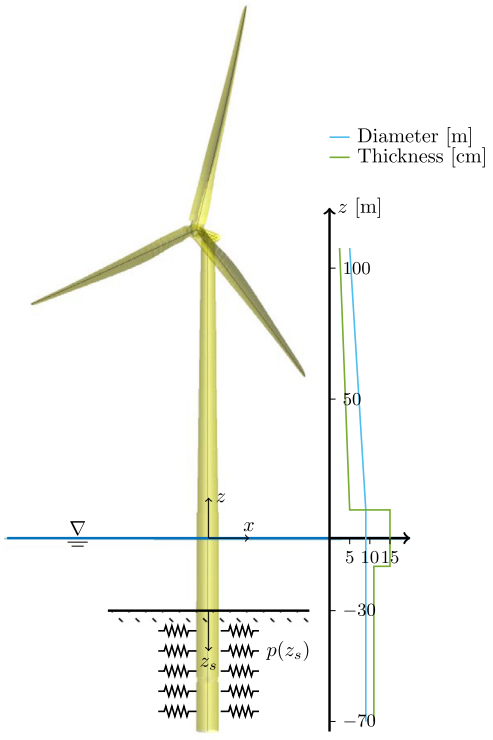

Fig. 2. Numerical model. Diameter is varying from 5.4 m in the top to 9.0 m at the bottom. Thickness varies between 38 and 150 mm.

periods are approximately 4.4 s, while the periods related to the second vibrational model are about 0.9 s in both directions. Consequently, the system is stiff, but still subjected to significant dynamic response from both wind and waves. The model has been validated in previous work, see e.g. [14]. The controller is an extended version of [15] with the possibility of increasing the fore-aft aerodynamic damping and avoid rotational speeds coinciding with the natural periods of the system. For integration in time-domain and calculation of aerodynamic loads, the finite-element method code USFOS/vpOne is used [16,17], while the hydrodynamic loads are calculated by an external routine and imported to the FEM code on an equivalent wave kinematics grid for load calculation with the Morison equation. The method has been used as verified in previous studies (see [18–20]). The turbulent wind field is created with TurbSim [21] using the Kaimal spectrum and a turbulence intensity of 10%. For a parked/idling turbine, the blades are pitched to 82 degrees relative to the rotor plane, inducing only a slow rotation of the rotor.

4. Sub-populations

Due to several different states related to the turbine operation and downtime, an offshore wind turbine have sub-populations of significantly different response characteristics. Four different sub-populations are suggested, which are presented in Fig. 3 and defined as:

1. Operational turbine within operational wind speed limits
2. Parked turbine due to general unavailability independent of wind speed
3. Parked turbine due to wind exceeding the operational wind speed limit (25 m/s)
4. Parked turbine due to wind below the lower operational wind speed (4 m/s)

The fractions p_i satisfies $\sum_i p_i(\alpha) = 1$ for a given level of availability $\alpha \in [0, 1]$. Thus, the total fatigue damage can be found as:

$$D = \sum_i p_i D_i \tag{6}$$

Since the availability parameter α is independent of the response statistics from Monte Carlo simulations (MCS), it can be modelled as a random variable in the reliability analysis. Typically, the downtime of an offshore wind turbine is 4–10% [22,23] due to some failure, assumed to be uncorrelated with the environment. Hence, a probabilistic model of the availability using the beta distribution is introduced; $\alpha \sim \mathcal{B}[\mu_\alpha, \sigma_\alpha]$. The beta distribution is often used in modelling of the availability and corresponding costs in electrical systems [24] when both the failure rate and downtime are exponentially distributed [25]. Several distributions for component reliability are presented in e.g.

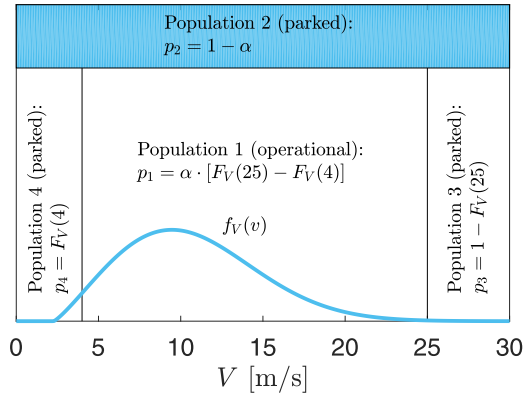

Fig. 3. Sub-populations, with fractions as functions of the wind speed marginal cumulative distribution F_V and an availability parameter α.

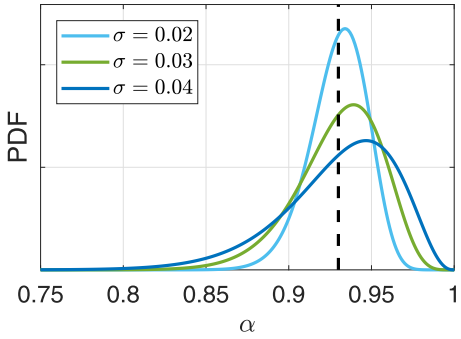

Fig. 4. Example beta-distributions for the availability parameter α, with $E[\alpha] = \mu = 0.93$. σ denotes the standard deviation in the beta-distribution.

Table 2
Population fractions and fatigue contribution coefficients (FCC) for $\alpha = 0.93$.

Population	p_i [%]	FCC_i [%]
1	89.6	76.0
2	7.0	21.0
3	0.1	2.6
4	3.3	0.4

Table 3
Stochastic variables for probabilistic analysis of fatigue damage. Note that an expected stress correction factor X_S of 1.5 is introduced to account for e.g. thickness variation, ovality and girth welds in the foundation [28].

Variable	Distribution	Expected value	Standard deviation
$\boldsymbol{\alpha}$	**Beta**	$\boldsymbol{\mu_\alpha}$	$\boldsymbol{\sigma_\alpha}$
Δ	Lognormal	1	0.3
s_0	Fixed	52.63	–
m_1	Fixed	3	–
m_2	Fixed	5	–
$\log K_1$	Normal	12.164	0.2
$\log K_2$	Normal	16.106	0.2
X_S	Lognormal	1.5	0.1
X_L	Lognormal	1.0	0.1
X_D	Normal	1.0	$\boldsymbol{\sigma_D}$
t_{ref}	Fixed	0.025	–
k	Fixed	0.2	–
ν_1	Normal	0.755	0.020
ν_2	Normal	0.262	0.005

[26] for wind turbine applications, one of which is the beta distribution. It is seen that the beta distribution is very flexible for modelling of failure rates compared to the Weibull, exponential and normal distributions. Hence, the beta distribution is chosen for the present work and examples of the stochastic modelling of α is shown in Fig. 4. Here, the uncertainty related to the choice of availability distribution is neglected. To underline the importance of modelling the availability, an example is shown in Table 2 for the individual populations considering the long-term fatigue damage at mudline for the presented model. The fatigue contribution coefficient (FCC) is defined as:

$$\text{FCC}_i = \frac{p_i \cdot E[D_i]}{\sum_j p_j \cdot E[D_j]} \tag{7}$$

and the example show that the FCC is significantly larger than the probability of occurrence for the unavailable population, p_2, meaning that a small variation in α may be amplified in the structural reliability analysis. As a consequence, durations where the turbine is parked will have a damage accumulation rate of almost four times that of a parked turbine, on average. The results throughout this paper are focusing on sub-populations 1 and 2 due to the domination over sub-populations 3 and 4 in fatigue damage contributions.

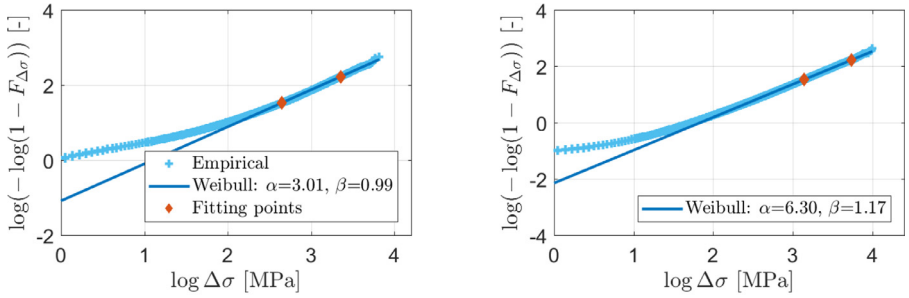

(a) Population 1 (b) Population 2

Fig. 5. A two-parameter Weibull distribution (solid line) is fitted to the simulated/empirical data (crosses) using two fitting point at $1 - F_{\Delta\sigma} = 10^{-2}$ and 10^{-4}.

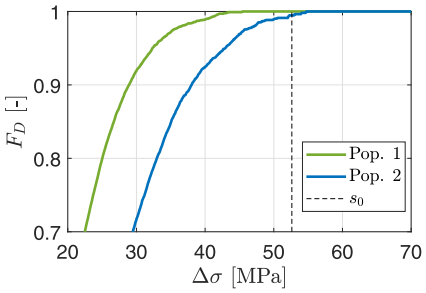

Fig. 6. Contributions to fatigue damage from sub-populations.

5. Fatigue damage estimation

The fatigue damage for the long-term stochastic environmental variables contained in $\mathbf{x}$ and the short-term random variables in $\boldsymbol{\epsilon}$, e.g. wave and wind component phases and amplitudes, is given as:

$$d(\mathbf{x}, \boldsymbol{\epsilon}) = \sum_{s \in \mathbf{s}(\mathbf{x},\boldsymbol{\epsilon})} \frac{s^{m_1}}{K_1}\mathcal{H}(s - s_0) + \frac{s^{m_2}}{K_2}\mathcal{H}(s_0 - s) \tag{8}$$

where $\mathbf{s} = \boldsymbol{\Delta\sigma}(t/t_{\text{ref}})^k X_S X_L$ is the rainflow-counted [27] stress ranges for a single stationary time-domain simulation with a duration of T_{sim} seconds, corrected for local plate thickness (t), stress uncertainty (X_S) and load model uncertainty (X_L). Furthermore, $\mathcal{H}$ is the Heaviside function, s_0 is the stress limit, the m's and K's are material parameters, and t_{ref} and k are constants to account for the plate thickness t. For probabilistic analysis, uncertainty in the SN-curve is accounted for by introducing a mean and variance on $\log K_{1,2}$ [28]. The short-term variability can be overcome by M repeated simulations with different seeds, i.e. uncorrelated sampling of $\boldsymbol{\epsilon}$ for a given $\mathbf{x}$. Some other aspects of reducing the short-term variability are discussed in [29] with a probability-based approach, and in [30] with emphasis on simulation length. The 1-year fatigue damage for the variables in $\mathbf{x}$ is found with:

$$d(\mathbf{x}) = \frac{365 \cdot 24 \cdot 3600}{M \cdot T_{\text{sim}}} \cdot \sum_{i=1}^{M} d(\mathbf{x}, \boldsymbol{\epsilon}_i) \tag{9}$$

With reference to Eq. (9), industry standards [31] recommend that either $M = 6$ and $T_{\text{sim}} = 600$s, or $M = 1$ and $T_{\text{sim}} = 3600$s to predict sufficiently accurate short-term results. In this work, focus is on evaluating the long-term fatigue, which can be expressed as an integral over the dimensions in $\mathbf{x}$:

$$D = \int_{-\infty}^{\infty} d(\mathbf{x}) \cdot f_{\mathbf{X}}(\mathbf{x}) d\mathbf{x} \tag{10}$$

which evaluated using N Monte Carlo simulations is simply the arithmetic mean:

$$D^{\text{mcs}} = \frac{1}{N}\sum_{i=1}^{N} d(\mathbf{x}_i) \tag{11}$$

To limit the scope of this paper, no importance sampling or other means of variance reduction techniques are used for the long-term fatigue estimate, and $d(\mathbf{x})$ will be evaluated according to Eq. (9) with $M = 1$ and $T_{\text{sim}} = 600$.

6. Reliability analysis

In this study, the foundation fatigue is the only considered contribution to the structural reliability. Then, the failure probability for n years of operation is:

$$p_f = P\left[\Delta \leq n \sum_i p_i D_i\right] \tag{12}$$

where $\Delta \sim \text{Logn}[1.0, 0.3^2]$ (as suggested in [32]) is accounting for the uncertainty in the Palmgren–Miner summation of the rainflow-counted stress cycles, and D_i is the 1-year fatigue damage for sub-population i for a given structural component. It is important that the Miner sum uncertainty (Δ) is applied to the sum of all contributing populations. Finding the failure probability in each sub-population and then the union of failure in all populations would be non-conservative. The failure probability expressed as:

$$p_f = P[g \leq 0] \tag{13}$$

where $g = \Delta - n\sum p_i D_i$, can be evaluated by e.g. FORM/SORM

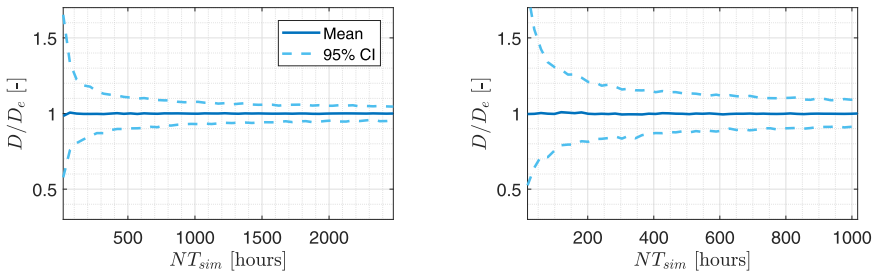

(a) Population 1 (b) Population 2

Fig. 7. Convergence of fatigue in dimensioning location at mudline as function of simulation hours. D_e is the expected fatigue damage.

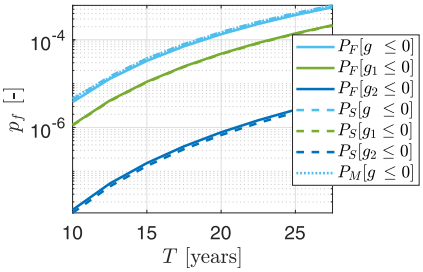

Fig. 8. Failure probability for system(g), sub-population 1 (g_1) and sub-population 2 (g_2). Subscript F represents FORM calculation, S denotes SORM, and M is MCS. The failure probability is for $\mu_\alpha = 0.94$ and $\sigma_\alpha = 0.04$.

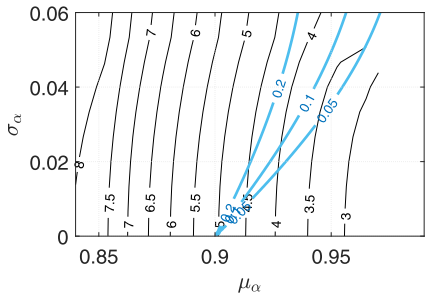

Fig. 9. Cumulative failure probability for $n = 25$ years normalised with 10^{-4}, for the beta-distributed availability with variation in mean (μ_α) and standard deviation (σ_α). In blue: $P[\alpha < 0.90]$. (For interpretation of the references to colour in this figure legend, the reader is referred to the web version of this article.)

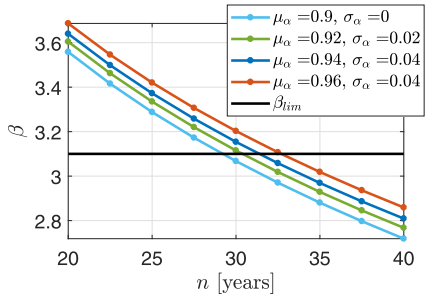

Fig. 10. Increased reliability index β for different stochastic models of α.

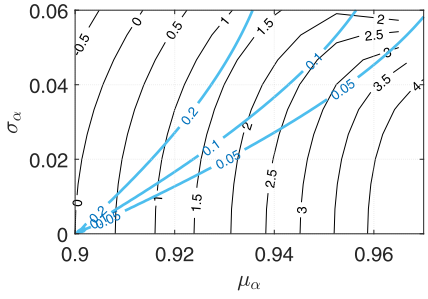

Fig. 11. Increased lifetime in years compared to deterministic $\alpha = 0.90$. Blue lines for $P[\alpha < 0.90] \in [0.05, 0.1, 0.2]$. (For interpretation of the references to colour in this figure legend, the reader is referred to the web version of this article.)

analysis [33] or Monte Carlo simulations. The reliability index denoted β is frequently used in this paper, which is a measure of the shortest distance to the failure surface. For the FORM analysis, the reliability index β is:

$$\beta_{\text{FORM}} \approx -\Phi^{-1}(p_f) \tag{14}$$

6.1. Uncertainty from SN-curve

If the uncertainty in the SN-curve is to be accounted for, the reliability is traditionally performed with the Weibull-distributed long-term stress range as a basis for the fatigue damage [32,34]. The fatigue damage from a Weibull distributed stress range; $\Delta\sigma \sim \text{Weibull}[a,\ b]$, yields the closed-form solution [35]:

$$D_i = \nu_i\, T\, X_D \left\{ \frac{[\,a_i X_S X_L\,(t\,/\,t_{\text{ref}})^k\,]^{m_1}}{K_1} \Gamma\left[1 + \frac{m_1}{b_i}, \left(\frac{s_0}{a_i}\right)^{b_i}\right] + \frac{[\,a_i X_S X_L\,(t\,/\,t_{\text{ref}})^k\,]^{m_2}}{K_2} \gamma\left[1 + \frac{m_2}{b_i}, \left(\frac{s_0}{a_i}\right)^{b_i}\right] \right\} \tag{15}$$

for sub-population i, where $\Gamma[\cdot,\ \cdot]$ and $\gamma[\cdot,\ \cdot]$ are the upper incomplete gamma functions and incomplete gamma functions, respectively. Furthermore, X_D is the fatigue uncertainty related to number of MCS, T is one year in seconds and ν is the sub-population dependent mean stress cycle rate found from simulations. An overview of the stochastic and deterministic parameters used in the reliability analysis is given in Table 3. The SN-curve used is the curve denoted D in [28] for steel in seawater with cathodic protection. The variance on the material parameters $\log K_1$ and $\log K_2$ are suggested in [28]. Furthermore, the standard deviation on the stress uncertainty X_S and load model uncertainty X_L is chosen as 0.1, partly based on [36,37].

Although the response characteristics in the present case do not yield a perfectly Weibull distributed stress range. In Fig. 5, example Weibull fits are shown. A 2-parameter Weibull distribution is fitted to the distribution tail using two fitting points in the upper range of the data. The fatigue damage error using the fitted Weibull stress range and direct evaluation of the Palmgren–Miner was found to be less than 5% in all cases. For fatigue calculations, it is important that the stress range representation is correct for the stress ranges that contribute the most to the total fatigue damage. As indicated in Fig. 6, the fatigue damage derived from approximately $\Delta\sigma > 10$ [MPa] or $\log\Delta\sigma > 2.3$ is dominating, meaning that the Weibull fit should be accurate in this range. Hence, it is assumed that the 2-parameter Weibull with tail weighting is sufficient in all present cases to satisfy this requirement. Also, the advantage with 2-parameter Weibull is the closed-form solution to the Palmgren-Miner summation as presented in Eq. (15).

7. Results

In this section, the convergence of fatigue damage, foundation reliability and the impact of the availability model on the structural reliability is presented. The fatigue damage and failure probabilities are given at the most critical circumferential location in the foundation at sea-bed level.

7.1. Fatigue damage convergence

For each sub-population, simulations are performed until a user-specified convergence criteria is met as illustrated in Fig. 7. When a satisfying confidence interval is obtained, a probabilistic model of the stress range can be established as described above. By assuming a normally distributed X_D to account for uncertainty in fatigue damage related to the number of MCS, the following relation is found:

$$\sigma_{D_1} \approx 4.62\, N^{-0.63} \tag{16a}$$

$$\sigma_{D_2} \approx 3.17\, N^{-0.49} \tag{16b}$$

Note that the convergence in sub-population 1 is faster than in sub-population 2, due to slightly smaller response variability. For the presented results, no uncertainty related to fatigue damage convergence is accounted for, meaning that $N \to \infty$ and $\sigma_D = 0$ for both sub-populations. Furthermore, as seen in Fig. 6, accumulated fatigue in the foundation is dominated by low-amplitude stress ranges in both sub-

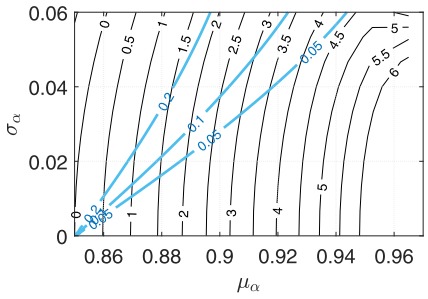

Fig. 12. Increased lifetime in years compared to deterministic $\alpha = 0.85$. Blue lines for $P[\alpha < 0.85] \in [0.05, 0.1, 0.2]$. (For interpretation of the references to colour in this figure legend, the reader is referred to the web version of this article.)

populations. In practice, only the high-cycle part of the SN-curve with $m = 5$ is utilised.

7.2. Combined failure probability

With reference to Fig. 8 it is found that all three methods give similar results, although the SORM method is slightly closer to the MCS solution than FORM. The total failure probability is significantly higher than the direct summation of the failure probabilities in sub-populations 1 and 2 due to a large number of shared stochastic variables related to the SN-curve, Miner sum and other uncertainties.

7.3. Impact on reliability and lifetime estimate

In Fig. 9, results from a parameter study of the beta-distributed availability are presented. Using common practice, there is no uncertainty in the availability and a characteristic value of 0.9 is used [1]. This corresponds to a beta-distribution with mean value of 0.9 and zero standard deviation. The figure shows how the estimated failure probability changes with different availability distributions. For instance, the accumulated failure probability can be reduced from $5{\cdot}10^{-4}$ with the deterministic model to $3.6{\cdot}10^{-4}$ if a mean value of 0.94 and standard deviation of 0.04 are used. With this availability model, we can read from Fig. 9 that there is a 10% probability that the availability is less than 0.9. It can be interpreted as if 10% of the turbines in a farm will have an availability of 0.9 or less. With a deterministic model, it is assumed that every single turbine has an availability of 0.9. The results show that a deterministic availability model is likely to yield pessimistic lifetime estimates.

In Fig. 10, the temporal evolution of the reliability index β is shown for several models for the beta-distributed availability. The additional lifetime is then calculated based on the difference between time before down-crossing of $\beta_{lim} = 3.1$ - the reliability index corresponding to a cumulative failure probability of 10^{-3}, and the lifetime using deterministic availability. Fig. 11 shows the additional lifetime compared to 90% deterministic availability as a function of the stochastic availability model. Isoquants for $P[\alpha < 0.90]$ indicate combinations of μ_α and σ_α which have the same probability of superseding 90% availability. For instance, choosing a stochastic model of the availability with a mean of 94% and 10% probability of being below 90% ($P[\alpha < 0.90] = 0.1$]), an additional 2.3 years of expected lifetime is obtained. For comparison, a similar study using a deterministic availability of 85% is shown in Fig. 12. By investigating the isoquant for $P[\alpha < 0.85] = 0.1$ and comparing with Fig. 11, it is clear that there is a slight benefit using the stochastic modelling for lower values of the deterministic availability.

8. Conclusion

The framework presented in this paper allows for the availability of an offshore wind turbine to be modelled as a stochastic variable, and thus reducing the failure probability and increasing the operational lifetime. An increase of approximately 10% in operational lifetime is proven for the present case if a deterministic availability of 90% is replaced with a beta-distributed availability model using expected availability of 94% and a standard deviation of 4%. In other words, the duration of assumed lost power production using a deterministic availability of 90% can almost be reclaimed by performing a reliability analysis, depending on the distribution of α.

As wind turbines in the same wind farm will most likely experience different downtime portions, the presented approach is useful for preventing unintentional design conservatism. Also, having fatigue response models for the different sub-populations may prove useful for estimates of remaining useful lifetime when using the actual availability from monitoring of the turbines.

Acknowledgements

This work has been carried out at the Centre for Autonomous Marine Operations and Systems (NTNU AMOS). The Norwegian Research Council is acknowledged as the main sponsor of NTNU AMOS. This work was supported by the Research Council of Norway through the Centres of Excellence funding scheme, Project number 223254 - NTNU AMOS.

References

[1] DNV GL. Loads and site conditions for wind turbines. 2016.
[2] Velarde J, Bachynski EE. Design and fatigue analysis of monopile foundations to support the DTU 10 MW offshore wind turbine. Energy Procedia 2017;137:3–13. https://doi.org/10.1016/j.egypro.2017.10.330.
[3] Schløer S, Bredmose H, Bingham HB. The influence of fully nonlinear wave forces on aero-hydro-elastic calculations of monopile wind turbines. Marine Struct 2016;50:162–88. https://doi.org/10.1016/j.marstruc.2016.06.004.
[4] Ziegler L, Voormeeren S, Schafhirt S, Muskulus M. Sensitivity of wave fatigue loads on offshore wind turbines under varying site conditions. Energy Procedia 2015;80:193–200. https://doi.org/10.1016/j.egypro.2015.11.422.
[5] Kvittem MI, Moan T. Frequency versus time domain fatigue analysis of a semi-submersible wind turbine tower. Proceedings of the 33rd international conference on ocean, offshore and arctic engineering. 2014.
[6] Zwick D, Muskulus M. Simplified fatigue load assessment in offshore wind turbine structural analysis. Wind Energy 2016;19:265–78.
[7] Low YM. A variance reduction technique for long-term fatigue analysis of offshore structures using Monte Carlo simulation. Eng Struct 2016;128:283–95. https://doi.org/10.1016/j.engstruct.2016.09.047.
[8] DNV GL. PROBAN – general purpose probabilistic analysis program. 1996.
[9] Horn J-T, Krokstad JR, Amdahl J. Long-term fatigue damage sensitivity to wave directionality in extra large monopile foundations. J Eng MaritEnviron 2018;232:37–49. https://doi.org/10.1177/1475090217727136.
[10] Reistad M, Breivik Ø, Haakenstad H, Aarnes OJ, Furevik BR, Bidlot JR. A high-resolution hindcast of wind and waves for the north sea, the Norwegian sea, and the Barents sea. J Geophys Res 2011;116(5):1–18. https://doi.org/10.1029/2010JC006402.
[11] Horn J-T, Bitner-Gregersen EM, Krokstad JR, Leira BJ, Amdahl J. A new combination of conditional environmental distributions. Appl Ocean Res 2018;73:17–26.
[12] Bak C, Zahle F, Bitsche R, Yde A, Henriksen LC, Nata A, et al. Description of the DTU 10 MW reference wind turbine. Tech. Rep.. DTU; 2013.
[13] Bachynski EE, Ormberg H. Hydrodynamic modeling of large-diameter bottom-fixed offshore wind turbines. Proceedings of the ASME 34th international conference on ocean, offshore and arctic engineering. St. Johns, Canada: ASME; 2015.
[14] Sørum SH, Horn J-T, Amdahl J. Comparison of numerical response predictions for a bottom-fixed offshore wind turbine. Energy Procedia 2017;137:89–99. https://doi.org/10.1016/j.egypro.2017.10.336.
[15] Hansen MOL. Aerodynamics of wind turbines. 2nd ed. 2013. 9781849770
[16] Hansen MOL, Holmås T, Aas-Jakobsen K, Amdahl J. vpOne – a new FEM based servo-, hydro- and aeroelastic code for wind turbines. Offshore wind energy. 2009.
[17] Popko W, Vorpahl F, Zuga A, Kohlmeier M, Jonkman J, Robertson A, et al. Offshore code comparison collaboration continuation (OC4), phase I – results of coupled simulations of an offshore wind turbine with jacket support structure. J Ocean Wind Energy 2013;1(1):1–11.
[18] Horn J-T, Krokstad JR, Amdahl J. Hydro-elastic contributions to fatigue damage on a large monopile. Energy Procedia 2016;94:102–14.
[19] Baekkedal E.. Alternative methods for realizing the sea spectrum for time-domain simulations of marine structures in irregular seas. 2014.
[20] Horn J-T. Stochastic dynamic analysis of offshore bottom-fixed structures. Tech. Rep.. NTNU/AMOS; 2015.
[21] Kelley N, Jonkman B. Overview of the TurbSim stochastic inflow turbulence

simulator. Tech. Rep.. 2007.
[22] GL Garrad Hassan. A guide to UK offshore wind operations and maintenance. Tech. Rep.. Scottish Enterprise and The Crown Estate; 2013.
[23] Faulstich S, Hahn B, Tavner PJ. Wind turbine downtime and its importance for offshore deployment. Wind Energy 2011. https://doi.org/10.1002/we.421.
[24] Sauvé J, Rebouças R, Moura A, Bartolini C, Boulmakoul A, Trastour D. Business-driven decision support for change management: planning and scheduling of changes. Proceedings of the 17th IFIP/IEEE international conference on distributed systems: operations and management. Berlin, Heidelberg: Springer-Verlag; 2006. p. 173–84.
[25] Abramowitz M, Stegun IA. Handbook of mathematical functions. 1965.
[26] Scheu MN, Kolios A, Fischer T, Brennan F. Influence of statistical uncertainty of component reliability estimations on offshore wind farm availability. Reliab Eng Syst Saf 2017:1–12. https://doi.org/10.1016/j.ress.2017.05.021.
[27] Downing SD, Socie DF. Simple rainflow counting algorithms. Int J Fatigue 1982;4(1):31–40.
[28] DNV GL. RP-C203 fatigue design of offshore steel structures. 2005.
[29] Horn J-T, Jensen JJ. Reducing uncertainty of Monte Carlo estimated fatigue damage in offshore wind turbines using FORM. Practical design of ships and other floating structures – PRADS. 2016. Copenhagen
[30] Zwick D, Muskulus M. The simulation error caused by input loading variability in offshore wind turbine structural analysis. Wind Energy 2015;18(8). https://doi.org/10.1002/we.1767.
[31] DNV GL. OS-J101 design of offshore wind turbine structures. 2014.
[32] DNV GL. RP-C210 probabilistic methods for planning of inspection for fatigue cracks in offshore structures. 2015.
[33] Madsen H, Krenk S, Lind N. Methods of structural safety. Prentice-Hall, Inc.; 1986.
[34] Ayala-Uraga E, Moan T. Fatigue reliability-based assessment of welded joints applying consistent fracture mechanics formulations. Int J Fatigue 2007;29(3):444–56. https://doi.org/10.1016/j.ijfatigue.2006.05.010.
[35] Nolte K, Hansford J. Closed-form expressions for determining the fatigue damage of structures due to ocean waves. Society of petroleum engineers journal. 17. 1977. p. 431–40. https://doi.org/10.2118/6250-PA.
[36] Sørensen JD. Reliability assessment of wind turbines. 12th international conference on applications of statistics and probability in civil engineering, ICASP12, Vancouver, Canada. 2015.
[37] Ambühl S, Ferri F, Kofoed JP, Sørensen JD. Fatigue reliability and calibration of fatigue design factors of wave energy converters. Int J Marine Energy 2015;10:17–38. https://doi.org/10.1016/j.ijome.2015.01.004.